SPONTANEOUS RAMAN SCATTERING AS A HIGH RESOLUTION XUV RADIATION SOURCE

by

J.E. Rothenberg, J.F. Young, and S.E. Harris

Preprint

G.L. Report No. 3539

January 1983

supported by

Contract F49620-80-C-0023

and

NASA NAG 2-44

Edward L. Ginzton Laboratory
W.W. Hansen Laboratories of Physics
Stanford University
Stanford, CA 94305

SPONTANEOUS RAMAN SCATTERING AS A HIGH RESOLUTION XUV RADIATION SOURCE*

by

Joshua E. Rothenberg,† J. F. Young, and S. E. Harris
Edward L. Ginzton Laboratory
Stanford University
Stanford, California 94305

ABSTRACT

The paper describes a new type of high resolution XUV radiation source which is based upon spontaneous anti-Stokes scattering of tunable incident laser radiation from atoms excited to metastable levels. The theory of the source is summarized and two sets of experiments using He $(1s2s)^1S$ atoms, produced in a cw hollow cathode and in a pulsed high power microwave discharge, are discussed. The radiation source is used to examine transitions originating from the $3p^6$ shell of potassium. The observed features include four previously unreported absorption lines and several sharp interferences of closely spaced autoionizing lines. A source linewidth of about 1.9 cm^{-1} at 185,000 cm^{-1} is demonstrated.

*The work described here was supported by the Air Force Office of Scientific Research, the Army Research Office, and the National Aeronautics and Space Administration.

†Present address: IBM Watson Research Center, P.O. Box 218, Yorktown Heights, New York 10598.

SPONTANEOUS RAMAN SCATTERING AS A HIGH RESOLUTION XUV RADIATION SOURCE

by

Joshua E. Rothenberg, J. F. Young, and S. E. Harris
Edward L. Ginzton Laboratory
Stanford University
Stanford, California 94305

I. INTRODUCTION

Recent interest in extreme ultraviolet (XUV) physics has created a demand for extremely high resolution spectroscopic tools in this spectral region. Studies of autoionization and Rydberg series in atoms, as well as in molecular spectra, have shown important structure on the scale of 1 cm^{-1} [1].

To reach this resolution at 500 Å, where 1 Å is equivalent to 400 cm^{-1}, requires an instrumental linewidth of 2.5 mÅ, or a resolving power of 200,000. A 10-meter monochromator with an aberration free, 6000 ℓ/mm grating would attain this resolution at a slit width of 15 μm. The lack of availability of such instruments, along with the difficulties of low throughput and order sorting has made an alternative approach desirable. In this paper we report the development of a new radiation source in the XUV [2] and its application to high resolution spectroscopy [3,4].

The radiation source is based upon spontaneous Raman scattering [5,6] of incident laser photons from excited metastable atoms. The metastable atoms may be produced in a discharge; in this work both cw hollow cathode and high power pulsed microwave discharges are used. Metastable atoms may also be produced with a pulsed hollow cathode discharge [7] or, as recently demonstrated [8], by photoionization of ground level atoms by soft x-rays from a laser produced plasma.

The upper and lower sidebands of the scattered radiation have frequencies equal to the sum and difference, respectively, of the metastable storage frequency and the frequency of the incident laser photon. By tuning the frequency of the incident laser, the frequency of the scattered radiation is tuned. Each sideband has a linewidth equal to the convolution of the incident laser linewidth and the Doppler width of the radiating atoms. The accessible spectral range is therefore determined by the range of available tunable lasers, and by the number of species which may be used for metastable storage.

The spontaneous Raman radiation is only generated while the pump laser is present. Hence, the source may operate in a short pulse mode, and even on a picosecond time scale. If the storage and terminal states of the Raman process have zero angular momentum, and the pump laser is polarized, then the spontaneous Raman radiation will also be polarized.

In the following sections of this paper we first discuss the theory of the spontaneous Raman scattering source. Attention is given to intensity and saturation effects which limit its brightness. We then describe experimental work which, although limited to helium as the storage species, demonstrates the source as narrowband (resolution greater than 100,000 at 550 Å) and broadly tunable (spectral range of about 7,500 cm^{-1}). The source is used to examine transitions originating from the $3p^6$ shell of potassium. The observed features include four previously unreported narrow absorption lines and several sharp interferences of closely spaced autoionizing lines.

Finally, we consider the possibility of using the other inert gases, and also singly ionized column I metals for metastable storage. These species may allow a coverage of about 75% of the spectral region from 500 Å to 1500 Å.

II. THEORY

A. LINEAR SCATTERING CROSS SECTION

Figure 1 shows a partial energy level diagram of He. Energy is assumed to be stored in the He $1s2s\ ^1S$ metastable level at 20.6 eV. The initial level $|i\rangle$, is connected to the ground He $1s^2\ ^1S$ level $|f\rangle$ through a sum of intermediate levels $|n\rangle$ which have dipole allowed transitions to both the initial and final levels.

If a monochromatic pump field at frequency ω_p is applied to the system, the spontaneous Raman scattering of photons from metastable atoms can be visualized as a transfer of population to virtual levels at energies $\hbar(\omega_{if} \pm \omega_p)$ followed by spontaneous decay of this virtual population to the ground level $|f\rangle$. The process may be considered from either the point of view of an induced Einstein A coefficient, or of a linear scattering cross section. If N is the density (atoms/cm^3) of metastable storage atoms, then the number of XUV photons per sec which are scattered from a cm^3 of volume is

$$XUV_{photons/sec} = NA_{induced} = \frac{N\sigma_{spont}(P/A)_{pump}}{\hbar\omega_p} \qquad (1)$$

For laser pump intensities which are sufficiently low that saturation effects are not present, the differential scattering cross section for the upper sideband is given by

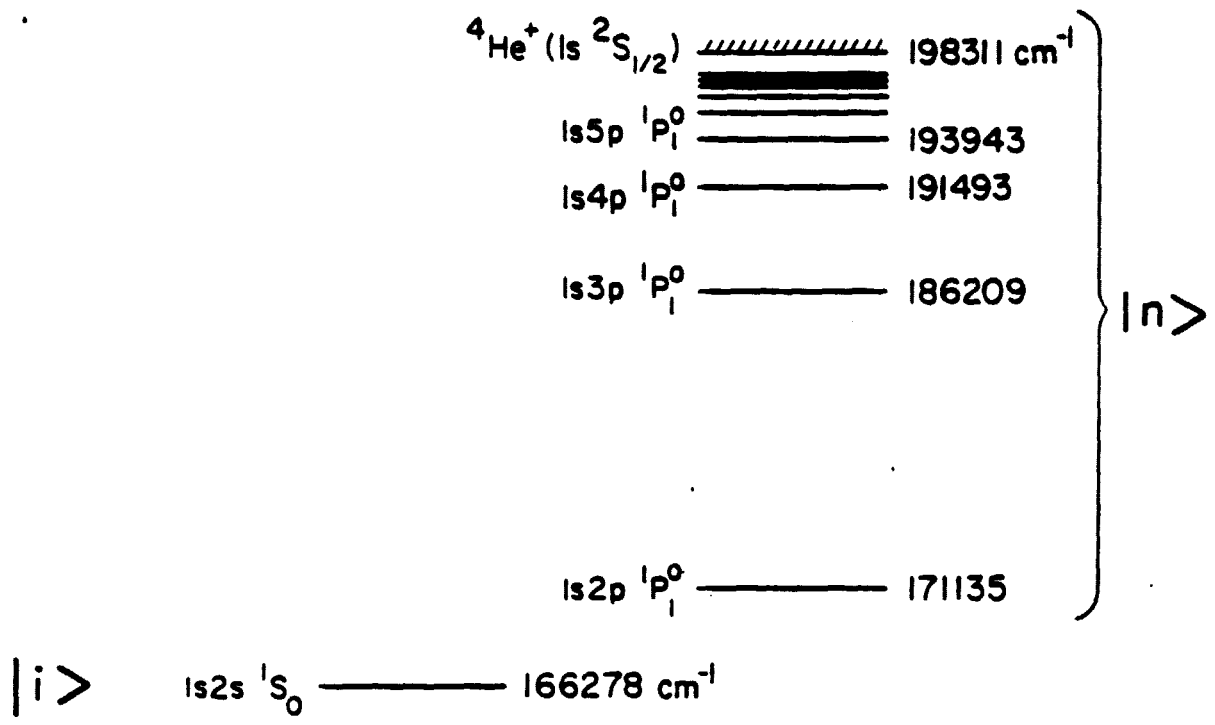

4838-11

Fig. 1--Atomic energy level diagram of ^4He.

$$\frac{d\sigma_{spont}}{d\Omega} = \frac{1}{16\pi^2}\,\frac{\omega_s^3\omega_p}{c^4\epsilon_0^2}\left|\sum_n \frac{\langle f|\vec{Q}\cdot\vec{\epsilon}_s^{\,*}|n\rangle\langle n|\vec{Q}\cdot\vec{\epsilon}_p|i\rangle}{E_n - E_f - \hbar\omega_s}\right.$$

$$\left. + \frac{\langle f|\vec{Q}\cdot\vec{\epsilon}_p|n\rangle\langle n|\vec{Q}\cdot\vec{\epsilon}_s^{\,*}|i\rangle}{E_n - E_i + \hbar\omega_s}\right|^2 \qquad (2)$$

where ω_s is the frequency of the scattered radiation ($\hbar\omega_s = E_i - E_f \pm \hbar\omega_p$), ω_p is the frequency of the pump photon, $\vec{\epsilon}_s$ and $\vec{\epsilon}_p$ are the respective polarization unit vectors, $\vec{Q} = -e\Sigma\vec{r}_i$ is the dipole moment operator for the atom, and E_i, E_n, and E_f are the energies of the initial, intermediate, and final states. The sum over intermediate states is performed over all dipole allowed transitions including the continua. To obtain the cross section for the lower sideband, simply replace $\vec{\epsilon}_p$ by $\vec{\epsilon}_p^{\,*}$ in Eq. (2). In the case of He, the upper sideband will have smaller resonance denominators, and therefore a significantly larger scattering cross section than does the lower sideband.

Figure 2 shows the upper sideband (anti-Stokes) scattering cross section [9] for He where the initial state is the metastable singlet level He $1s2s\ ^1S$, the final state is the ground level, and the intermediate levels are $|n\rangle = 1snp\ ^1P$ and the $1s\epsilon p\ ^1P$ continuum. The resonances are due to the intermediate levels $1s2p\ ^1P$ at 584 Å and $1s3p\ ^1P$ at 537 Å. As a result of both the ω_s^3 dependence of the scattering, and also of the relatively close approach to resonance, the per atom anti-Stokes scattering cross section in the XUV is often about six orders of magnitude larger than is typically encountered in the visible region of the spectrum.

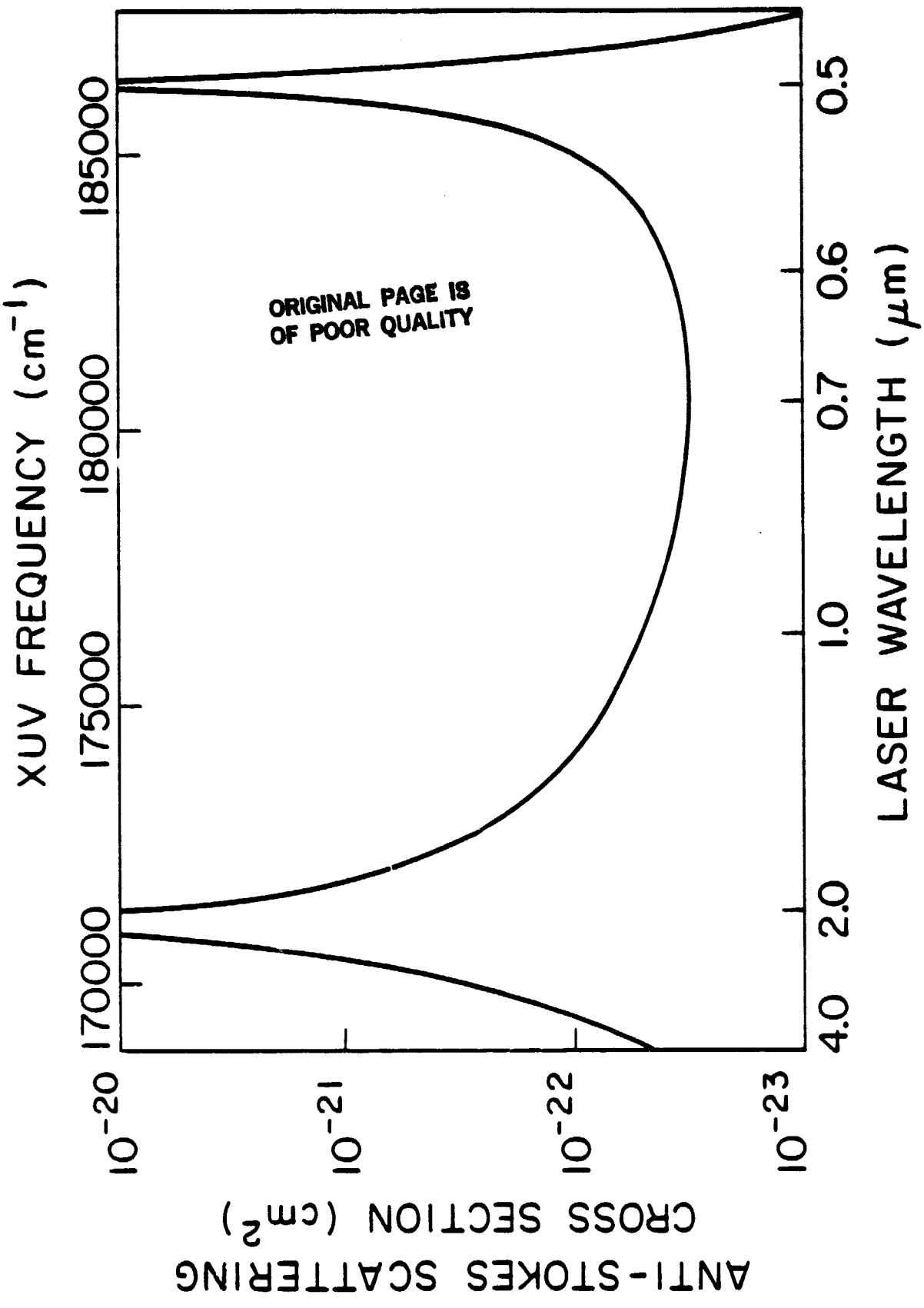

Fig. 2--Plot of anti-Stokes scattering cross section vs. tunable laser wavelength and scattered XUV frequency.

B. SATURATION

Three types of saturation of the anti-Stokes radiation source are typically encountered. These are: (1) simple depletion of the stored metastable population, (2) microscopic (per atom) saturation of the scattering process, and (3) macroscopic saturation, in the Planck equilibrium sense, of the emitting media.

1. Depletion

If we assume, as almost always will be the case, that the stored metastable population is not so large that the Raman scattering process represents a significant loss to the incident laser beam, then the laser pulse energy fluence which in essence scatters or depletes all of the stored population is

$$(J/A)_{saturation} = \frac{\hbar\omega_p}{\sigma_s} \qquad (3)$$

For a typical scattering cross section in He of $\sigma_s = 5 \times 10^{-23}$ cm^2, and ω_p corresponding to 6000 Å, this occurs at $J/A = 6.6 \times 10^3$ joules/cm^2. For beam size of several mm^2, as will most often be used in the spectroscopic applications of this source, this type of saturation is unlikely to be encountered.

2. Microscopic Saturation

As the incident laser power is raised, or a particular intermediate resonance is approached, all of the atoms in the storage level are in effect transferred to the virtual level and may then not radiate or scatter at a rate faster than the Einstein A coefficient of the approached intermediate

level. As this large field, or near resonance region, is approached, frequency shifts of the storage level and therefore of the scattered Raman radiation also occur, and may limit the resolution of the radiation source.

A simple and nearly exact solution of the near resonant problem is obtained from the dressed atom approach [10]. Defining the quantity θ by

$$\theta = \tan^{-1}\left(\frac{\mu_{in} E_p}{\hbar\Delta\omega}\right) \tag{4}$$

where μ_{in} and $\Delta\omega$ are the matrix element and detuning from the near resonant level $[\Delta\omega = \omega_n - (\omega_i + \omega_p)]$; the induced emission rate is

$$A_{induced} = \left(\frac{\omega_s}{\omega_{nf}}\right)^3 \sin^2\frac{\theta}{2} A_{nf} \tag{5}$$

and the frequency of the scattered anti-Stokes radiation is

$$\omega_s = (\omega_i - \omega_f) + \omega_p - \frac{\delta}{2} \tag{6a}$$

where

$$\delta = \Delta\omega\left(\frac{1 - \cos\theta}{\cos\theta}\right) \tag{6b}$$

When θ is small (low pump fields or large detunings), Eq. (5) reduces to a single term of Eq. (2).

3. Macroscopic Saturation

In a typical discharge or plasma the population of the final level (in He, the ground level) of the Raman process is often several orders of magnitude greater than the population of the metastable storage level. Incident

laser photons not only cause emission of XUV photons from the storage level, but also cause two-photon absorption of these same photons by atoms which are in the ground level. The interplay of the two-photon emission, i.e., the Raman emission, and the two-photon absorption yield a source brightness which is the same as that of a one-photon blackbody, except that the usual one-photon absorption coefficient is replaced by the two-photon absorption coefficient [2].

The brightness $B(\omega)$ (power per bandwidth in radians/sec per solid angle and area) for a sample of thickness L, is given by

$$B(\omega) = \frac{\hbar\omega^3}{8\pi^3c^2}\left[\frac{1}{(N_f/N_i) - 1}\right]\left[1 - e^{-(N_f - N_i)\sigma^{(2)}(\omega)L}\right] \qquad (7a)$$

$$\sigma^{(2)}(\omega) = \frac{8\pi^3c^2}{\omega^2}\,\frac{d\sigma_{spont}}{d\Omega}\,\frac{(P/A)_{pump}}{\hbar\omega_p}\,g(\omega) \qquad (7b)$$

where $\sigma^{(2)}$ is the two-photon absorption cross section for XUV radiation which results from the presence of the laser field ω_p. The lineshape $g(\omega)$ is the convolution of the initial (metastable) and final level lineshapes.

At frequencies or cell lengths where the column is two-photon opaque, the brightness of the spontaneous Raman radiation source is that of a blackbody at a Boltzmann temperature of the metastable level, i.e., $N_i/N_f = \exp[-(\hbar\omega_{if}/kT)]$. In the optically thin region where $N_f\sigma^{(2)}L \ll 1$, the brightness reduces to that obtained from the linear scattering cross section of Eq. (2).

III. EXPERIMENTAL RESULTS

A series of experiments was performed to demonstrate the use of spontaneous Raman scattering as a tunable high resolution source for absorption spectroscopy. The metastable helium $1s2s\ ^1S$ level was used as the Raman medium, producing radiation in the 500 Å spectral region (anti-Stokes upper sideband scattering). We used this source to examine potassium absorption features due to autoionizing transitions originating from the $3p^6$ shell. Two methods were used to excite helium atoms to the $1s2s\ ^1S$ storage level: a cw hollow cathode discharge and a high power pulsed microwave discharge. The first technique produced anti-Stokes radiation which was brighter than all other XUV emission from the plasma, thus simplifying detection; however, the radiation was relatively weak, thus limiting the tuning range. The second technique produced much larger anti-Stokes signals and greater tuning ranges, but the increased level of background XUV plasma emission mad the use of additional filtering necessary. Both methods are described below.

A. LOW CURRENT HOLLOW CATHODE DISCHARGE

A schematic of the basic apparatus is shown in Fig. 3. Helium metastable $1s2s\ ^1S$ population was produced in a 60 cm long hollow cathode discharge and a tunable dye laser (Nd:YAG pumped Quanta-Ray PDL-1) was directed down the discharge by a right-angle turning prism. Backward scattered anti-Stokes radiation passed by the prism (which obscured about one-half the aperture), through a potassium vapor cell, through an aluminum filter, and was incident on an electron multiplier tube.

The discharge consisted of a stainless steel cylindrical cathode 1.2 cm in diameter inside a concentric 2.5 cm stainless steel tube which served as

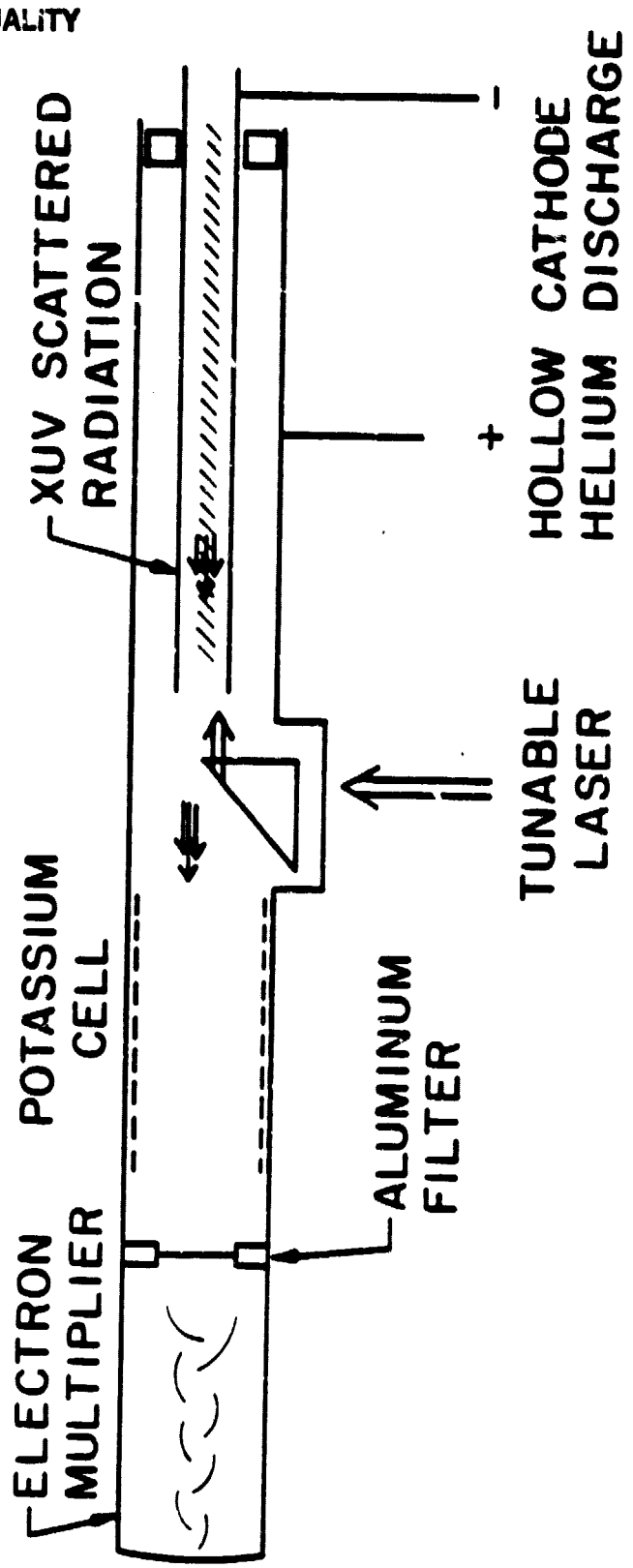

Fig. 3--Schematic of hollow cathode apparatus used for absorption spectroscopy of potassium.

the anode. The cathode had a slot 0.6 cm wide along the 60 cm active length of the discharge which allowed the glow to reside inside the cathode. Typical operating parameters of the discharge were 2 torr helium, 190 V, and 30 ma, which, based on previous measurements [11], implies a population of 1s2s ^{1}S metastables of about 10^{11} atoms/cm^3. The current through the discharge was kept low because it was found that the metastable population did not increase appreciably with current (up to a few hundred ma), but the background radiation from the plasma (predominantly resonance line radiation at 584 Å and 537 Å) increased linearly with the applied current. Thus, the largest signal-to-noise ratio was obtained at the lowest stable operating current of the discharge.

The potassium vapor cell consisted of a stainless steel tube 1.2 cm in diameter with a stainless steel wick. The active hot zone was 5 cm long and typically was operated at a potassium vapor density of 10^{15} atoms/cm^3 (260°C). The ambient helium discharge pressure slowed the diffusion of potassium both into the discharge and to the aluminum filter which served to separate the 2 torr helium pressure from the 10^{-6} torr operating pressure of the electron multiplier. Experiments were performed with potassium having a minimum purity of 98% and 99.95% with the same results.

The XUV photons transmitted through the potassium cell impinged directly upon the first dynode of an EMI D233 electron multiplier, liberating photoelectrons which were subsequently amplified in the remaining 13 stages of the tube. This fast linear focused tube provided single output pulse widths of ~ 5 ns and a gain of ~ 10^6 at an applied voltage of 3.7 kV. The output of the electron multiplier was processed with a fast preamplifier and a 10 ns wide gated integrator. A small computer digitized and recorded the resultant

voltage along with the input dye laser intensity. The computer also tuned the laser in steps of 0.048 Å.

For incident laser pulses of 50 mJ at 6000 Å we calculate that about 4.3×10^7 XUV photons per laser pulse are produced in the 60 cm long discharge at the anti-Stokes wavelength, 546.6 Å. The solid angle of the detector reduces the flux to 200 photons/pulse or (for the 10 pulse per second repetition rate) 2000 photons/sec. Thus, the ratio of the number of incident laser photons to the number of effective XUV photons is expected to be greater than 10^{14}. It is therefore essential to provide large discrimination against the visible laser photons. This was accomplished (1) by using a geometry which utilized backscattered XUV radiation, (2) by the $\sim 5 \times 10^{-8}$ rejection of the visible light by the aluminum filter, and (3) by the high work function of the electron multiplier. Even with these factors, if the incident laser reflected off an edge near the end of the discharge, the reflection overwhelmed the detected XUV photons. The transmittance of the aluminum filter (Luxel TF-101a, a 1500 Å thick film of Al alloyed with 1% silicon supported by a nickel mesh) is useful from ~ 850 Å to ~ 150 Å. At 550 Å approximately 10% of the incident flux is transmitted, whereas in the visible the filter is specified at less than 5×10^{-8} transmittance [12]. Therefore, we estimate the incident flux onto the detector at 200 photons/sec; assuming a detector quantum efficiency of 10% [13], we obtain a count rate of 20 counts/sec, which agrees well with our observations.

The spectral regions studied with this apparatus are shown in Table 1. Typical absorption scans are shown in Fig. 4. These scans are computer generated plots in which each point represents the sum of integrated signals from 5 laser settings, a total of 50 pulses covering ~ 0.75 cm^{-1}. The XUV

Table 1

Spectral Regions Studied with the

Hollow Cathode Discharge

Laser Dye	Range of Laser Wavelength (Å)	Range of XUV Frequency (cm^{-1})
Kiton Red 620	5990 - 5740	182975 - 183695
Rhodamine 590	5760 - 5470	183635 - 184549
Coumarin 500	5220 - 4880	185435 - 186769

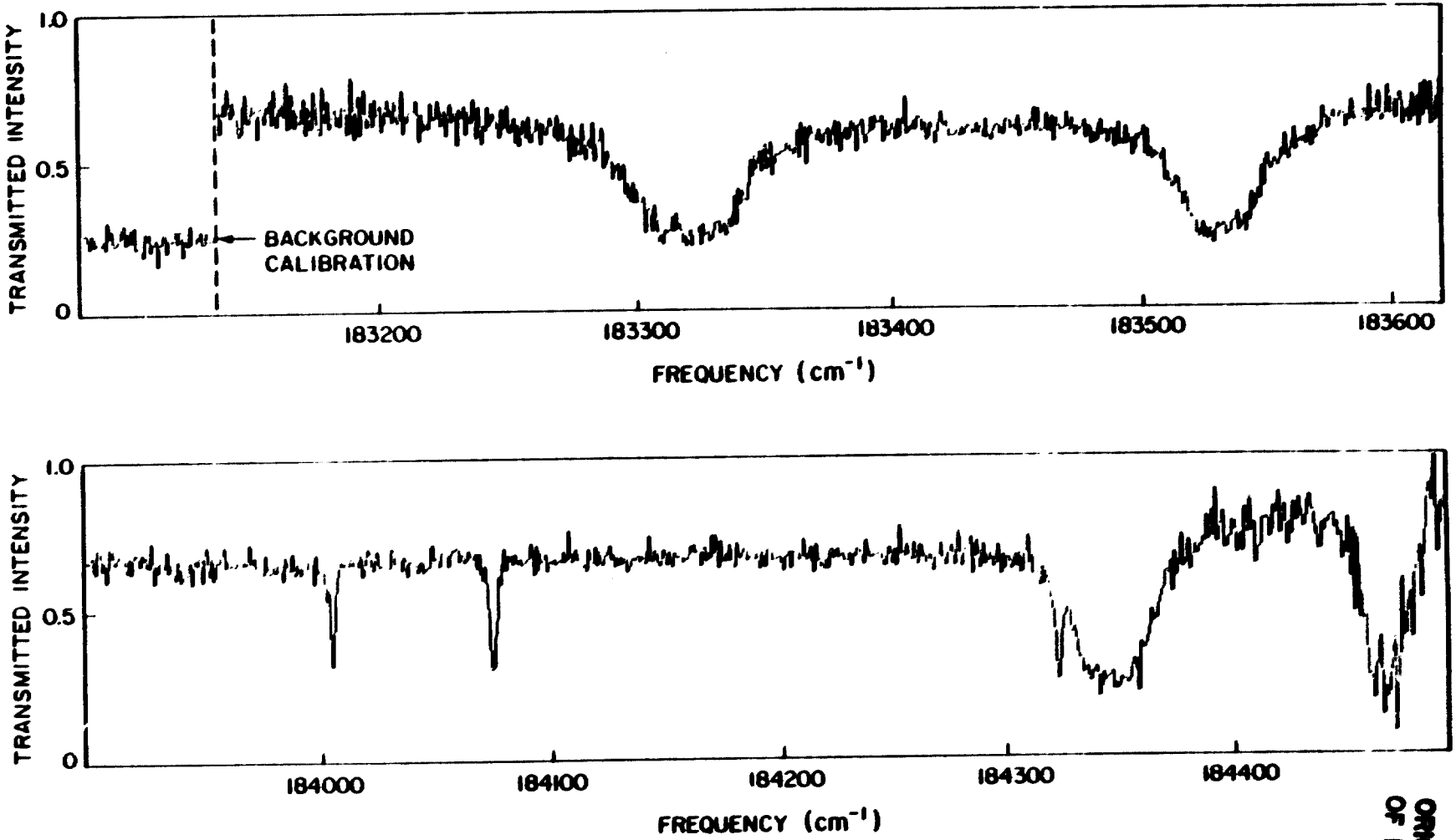

Fig. 4--Absorption scans of potassium obtained with hollow cathode apparatus. Potassium vapor density is 10^{15} atoms/cm^3, and cell length is 5.0 cm.

signal was normalized to the relative dye laser intensity, which has the effect of increasing the statistical fluctuation in regions of lower laser intensity.

The XUV frequency at each data point was obtained by adding the laser frequency to the frequency of the storage level, ^{4}He 1s2s ^{1}S, which has been accurately measured to be 166,277.55 ± 0.15 cm^{-1} [14,15]. The laser frequency was determined from the dial of the Quanta-Ray dye laser; this dial reading was calibrated using known Ne and Kr lines, and found to be resettable to ± 1 cm^{-1}.

Table 2 summarizes the energies and linewidths of the observed potassium absorption features. The broader features were observed by Mansfield [16], Mansfield and Ottley [17], and Kavei, et al. [18]. The narrower features have not been reported previously. We estimate that Mansfield [16] had an instrumental linewidth of approximately 40 cm^{-1} based upon microdensitometer traces he supplied. Thus, it is not surprising that weak lines a few cm^{-1} in width would escape detection. (Assuming that the linewidths of these features are about equal to that of the anti-Stokes radiation, a 50% absorption in Fig. 4 corresponds to an oscillator strength of $f = 3 \times 10^{-4}$.)

Our measured absorption linewidths were a function of the potassium vapor pressure, and the widths reported in Table 2 are the minimum full widths at half maximum obtained by reducing the cell pressure to a value at which negligible change in width was seen with further reduction. The narrowest observed absorption feature (at 185,806 cm^{-1}) had a measured width of 1.9 cm^{-1}, which approaches the theoretical linewidth of the anti-Stokes radiation, i.e., the convolution of the 0.3 cm^{-1} laser linewidth and the room temperature Doppler width of ~ 1.3 cm^{-1} of the emitting helium atoms [19].

Table 2

Potassium Absorption Features Observed with the Hollow Cathode Apparatus

Energy	Linewidth	Designation	Previously Observed Energy
183320 ± 1 cm^{-1}	8.4 cm^{-1}	$3p^5 3d(^3P)5s\ ^2P_{1/2}$	183322 [a] cm^{-1}
183530	10.5	$3p^5 3d(^3P)5s\ ^2P_{3/2}$	183532 [a]
184008	2.6		
184076	3.4		184076 [b]
184321	2.5		
184344	15.0	$3p^5 4s(^1P)5s\ ^2P_{3/2}$	184342 [a]
184465	7.8	$3p^5 4d(^3P)5s\ ^2P_{1/2}$	184471 [a]
185806	1.9		
186659	5.0	$3p^5 4d(^1D)4s\ ^2D_{3/2}$	186656 [a]

[a] M. W. D. Mansfield (1975) [Ref. 16].
[b] G. Kavei, et al. (1977) [Ref. 18].

Note that potassium vapor (at 260°C) has a Doppler width of ~ 0.5 cm^{-1} in this spectral region. A calculation which convolves the various linewidths involved shows that an observed 1.9 cm^{-1} linewidth implies a natural width of the line of ~ 0.5 cm^{-1}. This corresponds to an autoionizing time of ~ 10 ps, which is consistent with calculated autoionizing times for levels in potassium which are not allowed to autoionize to first order (in LS coupling) [20]. Thus, the narrow absorption lines are probably the result of transitions from the $3p^6 4s$ ground level to levels that, in the approximation of LS coupling, are forbidden by selection rules to autoionize, such as odd parity doublet series levels with even orbital angular momentum and levels in the quartet series.

As a result of the operation of the discharge at very low current, this apparatus had the inherent disadvantage of producing low signal levels. For a total of 50 pulses integrated per data point, we found that a dye laser energy of ~ 12 mJ/pulse was necessary to achieve an acceptable 3 to 1 signal-to-noise ratio. The spectral range that could be scanned in a reasonable time period (the scans shown in Fig. 4 took ~ 1-1/2 hours each to complete) was therefore limited to wavelengths generated using tunable radiation from the high output laser dyes. Thus, in order to investigate other spectral regions the inherent anti-Stokes signal level must be increased.

B. PULSED HIGH POWER MICROWAVE DISCHARGE

We made two changes to increase the brightness and thus the tuning range of the anti-Stokes radiation source: a high power microwave discharge was used to produce a larger population in the He 1s2s ^1S storage level, and the effective solid angle for collection of anti-Stokes radiation was improved.

The basic geometry is similar to that used previously and is shown in Fig. 5. Microwave pulses at 9.375 GHz, 2 μs long, with a peak power of about 500 kW were generated by a Varian SFD-303 coaxial magnetron and coupled into a 90 cm long, 4 mm i.d. quartz tube located inside a section of x-band waveguide, centered adjacent to the narrow wall. Helium gas at ~ 5 torr was flowed slowly through the tube. The helium broke down regularly during the rising edge of the microwave pulse; approximately 60% of the incident microwave energy was absorbed and less than 5% was reflected. Previous measurements [21] of microwave excited helium plasmas indicate that 1s2s ^{1}S storage level densities of about 10^{13} atoms/cm^3 are typically obtained, or about 100 times larger than achieved with the hollow cathode.

In addition, this apparatus collected a much larger fraction of the generated anti-Stokes radiation by making use of near-grazing incidence reflections of the XUV radiation at the inside surface of the quartz tube. At 500 Å, quartz reflects 90% of radiation incident at 88° [22], and the tube acts like a waveguide for these grazing rays. As illustrated in Table 3, the effective solid angle collection of such a tube can be larger by a factor of 10^2 - 10^3 than a similar geometry where there is no reflection of grazing rays. The second column of Table 3 shows the solid angle collected from a uniformly emitting source through a quartz tube of inside diameter 4 mm assuming no wall reflections, i.e., as if the tube were replaced by apertures at its ends. The third column shows the solid angle collected for the same geometry, except that the reflections are included. We note, however, that these reflections depolarize the initially polarized anti-Stokes radiation.

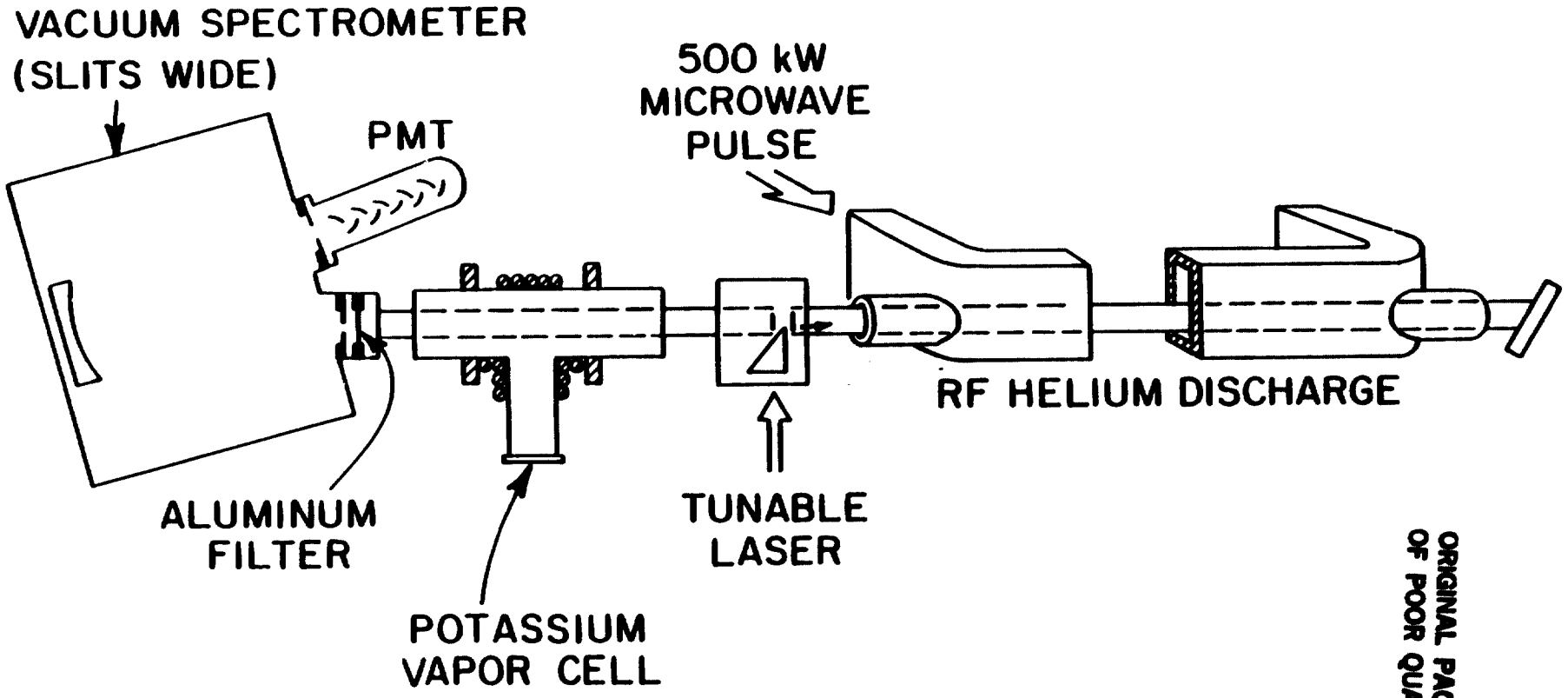

Fig. 5--Schematic of microwave pumped apparatus used for absorption spectroscopy of potassium.

Table 3

Collected Solid Angle Through a 4 mm Diameter Quartz Tube

Uniformly Illuminated at One End

Tube Length (cm)	Solid Angle Without Reflections (Steradians)	Solid Angle Including Reflections (Steradians)
10	1.2×10^{-3}	0.035
20	3.1×10^{-4}	0.019
50	5.0×10^{-5}	8.2×10^{-3}
100	1.2×10^{-5}	4.3×10^{-3}
200	3.1×10^{-6}	2.2×10^{-3}
400	7.8×10^{-7}	1.1×10^{-3}

The potassium vapor cell (Fig. 6) was redesigned so as to maintain the grazing reflection geometry. An alkali resistant glass tube was slotted (1 mm wide) to allow potassium vapor to permeate throughout, and a heater was wound on the glass tube to keep it hotter than the wet stainless steel wick, so as to prevent potassium condensation inside the tube. The potassium cell had an active hot zone 4.5 cm long. Over approximately 30 hours of operation, the potassium cell's throughput of XUV radiation decreased by a factor of 5. Apparently, this was due to contamination of and/or reactions on the inside surface of the glass tube, and a subsequent loss of reflectivity, since the throughput returned to its original value when the contaminated tube was replaced.

The main disadvantage in using the more intense microwave discharge was that the intensity of the spurious XUV radiation was much larger than the anti-Stokes signal intensity. The 584 Å integrated resonance line intensity was measured to be 15 times greater than the anti-Stokes intensity (using 50 mJ of laser energy at 6000 Å). As a result, it was necessary to filter the resonance radiation from the anti-Stokes radiation. A McPherson 225 one-meter normal incidence vacuum monochromator with a 1200 ℓ/mm grating ruled over a 30 mm × 50 mm area and coated with platinum was used in first order as a filter against the resonance radiation. The linear dispersion was 8.3 Å/mm, and the monochromator slit widths were set to discriminate against the nearest noise feature, while passing the desired range of anti-Stokes radiation. For the spectral range that we examined, the nearest noise feature was the second resonance line at 537.0 Å. Typically, the slits were set at a width of 0.8 - 1.0 mm, and thus, the resolution of the apparatus was due entirely to the spectral width of the anti-Stokes radiation.

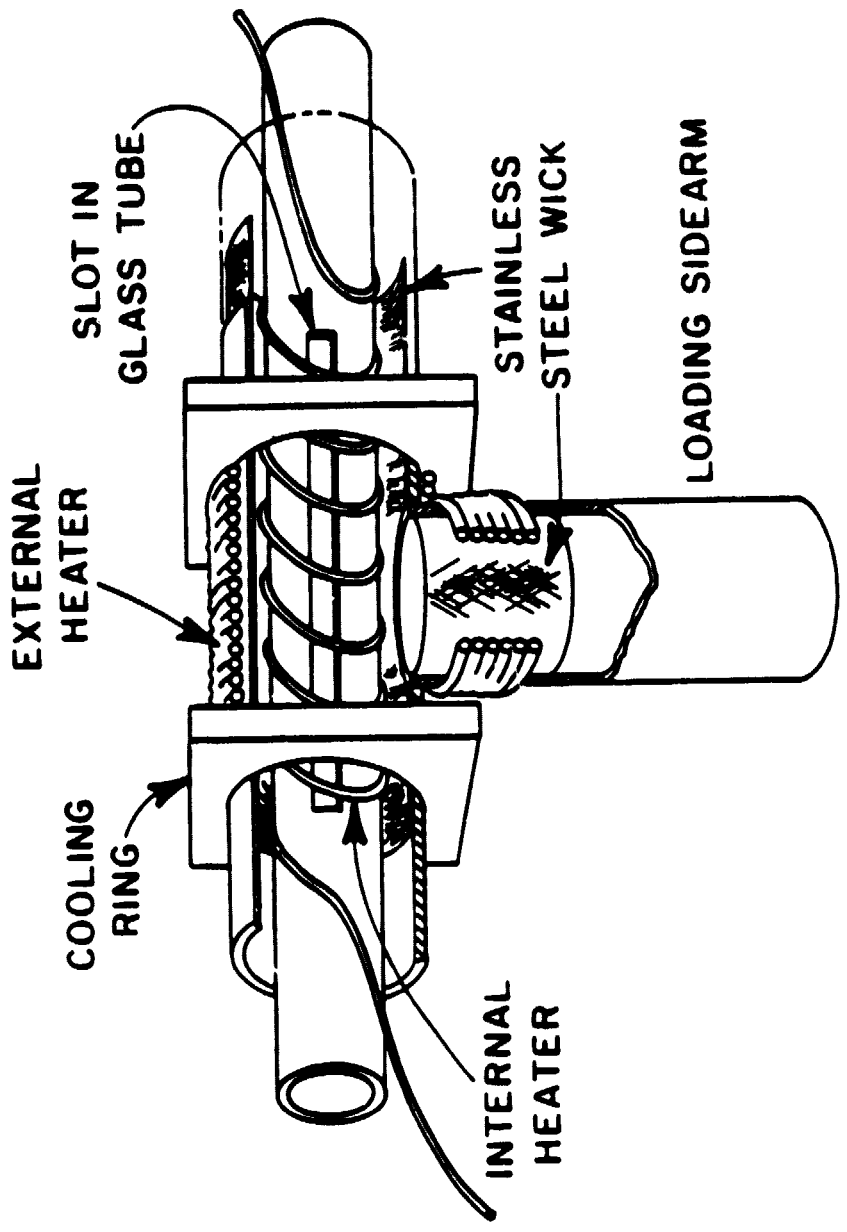

Fig. 6--Potassium vapor cell used with microwave apparatus.

The spectrometer, however, introduced a large throughput loss into the system. For an incident pulse energy of 25 mJ at 6000 Å through the helium plasma, we calculate that approximately 3.2×10^9 anti-Stokes photons are generated. Of these photons scattered into all directions, only an estimated 0.029%, or 9.3×10^5 photons emerge from the end of the potassium absorption cell. (Without the grazing-reflection collection this output would have been smaller by roughly 200.) Furthermore, the solid angle of the spectrometer reduces the collected flux by an additional factor of 15, the grating has an efficiency in the XUV of about 4%, and the aluminum filter transmits 10% of the anti-Stokes radiation. Thus, we estimate that about 250 photons strike the detector for each laser pulse. At ten laser pulses per second, this implies a flux of 2.5×10^3 photons/sec striking the detector, or for a 10% detector quantum efficiency, a net count rate of 250 per second. The observed count rate was ~ 200/sec, 10 times greater than with the hollow cathode.

The temporal behavior of the microwave excited discharge is shown in Fig. 7. The anti-Stokes radiation and resonance fluorescence intensities are proportional to their respective excited state populations. Thus, we conclude that in the first few hundred ns after breakdown (the avalanche period), the excited state populations reached their maximum value. For the duration of the microwave pulse, resonance fluorescence remained large, but the anti-Stokes radiation decreased to a small level. After the microwave pulse, recombination occurred in the cooling plasma, and both anti-Stokes radiation and resonance fluorescence regained intensity. The anti-Stokes radiation decayed during recombination with a time constant of ~ 4 μs, whereas resonance fluorescence decayed with a shorter time constant of

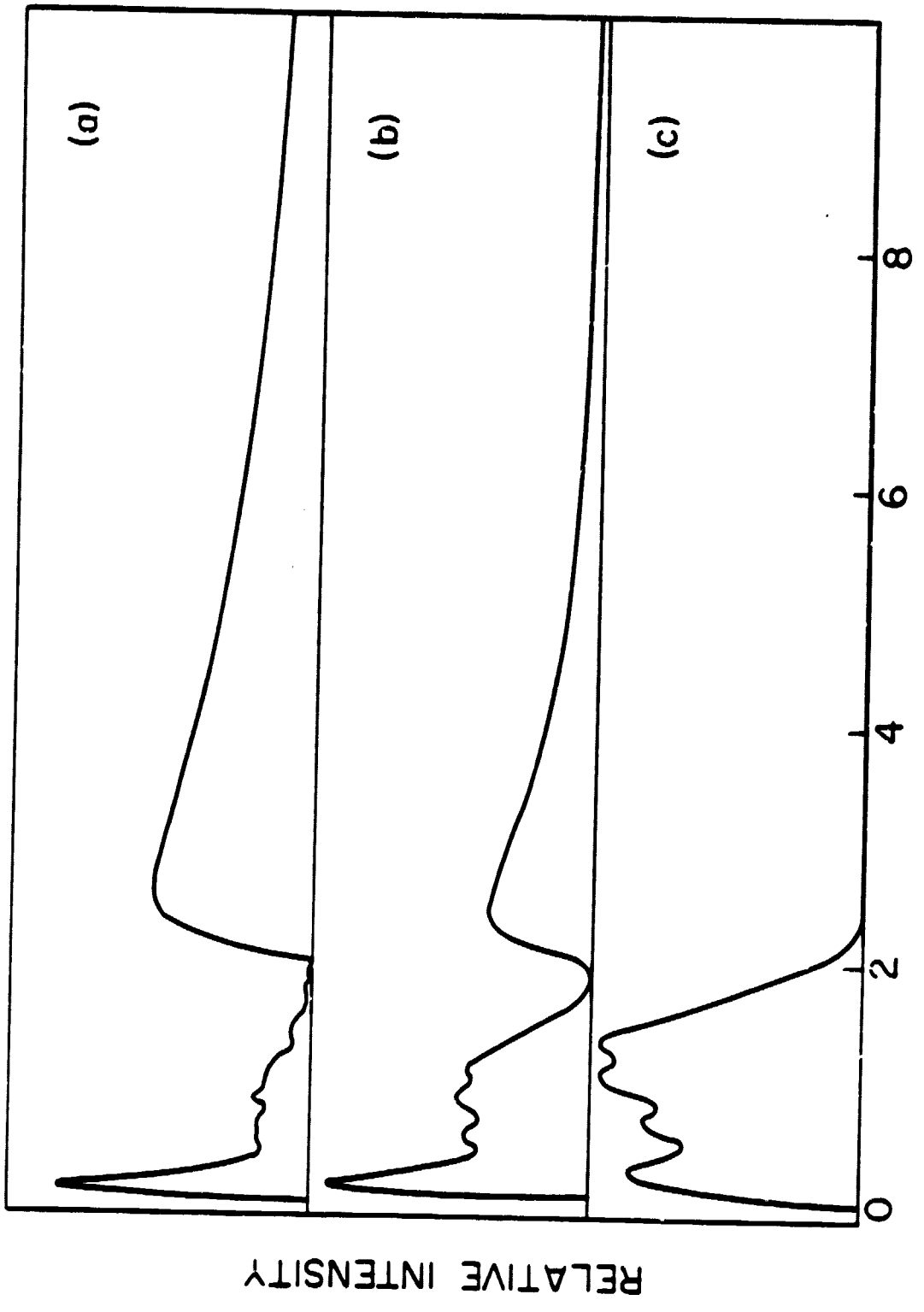

(4838-1)

Fig. 7--Temporal behavior of microwave discharge emission. (a) Anti-Stokes output at 550 Å, (b) resonance line emission at 584 Å, and (c) input microwave pulse.

~ 2 μs. Thus, the ratio of anti-Stokes intensity to resonance line intensity was largest in this recombination tail.

Unfortunately, operation late in the recombination period has a serious disadvantage. The measured widths of absorption features in potassium were about 2.5 cm^{-1} wider than measurements of the same features made during the avalanche period. We believe that this is due to an increase in the temperature of the metastables and hence, a larger Doppler width during the recombination period. The most likely mechanism for this heating is the elastic collisions of neutrals and ions with hot electrons, and the subsequent formation of hot metastables during the recombination period. From linewidth measurements during the recombination period we estimate that the Doppler width is 3.5 cm^{-1}, which implies an atomic kinetic temperature of ~ 3000°K (0.26 eV). The spectral width of the anti-Stokes radiation during the avalanche period was confirmed to be equal to that obtained with the hollow cathode discharge by measuring the linewidths of the same potassium absorption features. Because of this effect, all the measurements and spectra reported were made during the avalanche period.

Using the microwave discharge we extended the spectral region examined in potassium to 536.8 Å - 558.4 Å, as shown in Table 4. To achieve a signal-to-noise ratio of 3 to 1 with an integration of 50 laser pulses per point, a minimum of ~ 1 mJ of laser energy per pulse was required. Commercial sources of such energy per pulse are available to at least 2 μm, which implies a possible XUV spectral range of ~ 537 Å - 584 Å.

Table 5 lists a number of additional potassium absorption features we observed using the microwave excited discharge; all have been previously observed by Mansfield [16]. Typical absorption scans are shown in Fig. 8, which are computer generated plots containing 1024 points corresponding to laser

Table 4

Spectral Regions Studied with Microwave Excited

Anti-Stokes Radiation Source

Laser Dye	Range of Laser Wavelength (Å)	Range of XUV Frequency (cm^{-1})
Rhodamine 640	5960 - 6140	183055 - 182654
Sulforhodamine 640	6090 - 6180	182697 - 182458
DCM	6170 - 6690	182484 - 181224
Pyridine 1	6680 - 7220	181247 - 180127
Styryl 7	7210 - 7510	180146 - 179592
Styryl 8	7500 - 7800	179610 - 179098

Table 5

Linewidths and Positions of Potassium Absorption Features

Observed with the Microwave Apparatus

Energy (cm^{-1})	Linewidth (cm^{-1})	Designation	Previously Observed Energy (cm^{-1})
179885	4.0	$3p^5 3d(^3D)4s\ ^2D^o_{3/2}$ (a)	179886 (a)
179918	2.1		179920
180547	43.0	$3p^5 3d(^1P)4s\ ^2P^o_{1/2}$	180551
180794	55.0 (b)	$3p^5 3d(^1P)4s\ ^2P^o_{3/2}$	180791
180840	11.0 (b)		180850
181519	2.7		181517
181745	5.5	$3p^5 3d5s\ ^4P^o_{3/2}$	181742
182152	8.8		182152
182652	5.6		182651

(a) Energies and designations from Mansfield [Ref. 16].

(b) Lines very asymmetric; linewidths determined from fit to theoretical Fano profile.

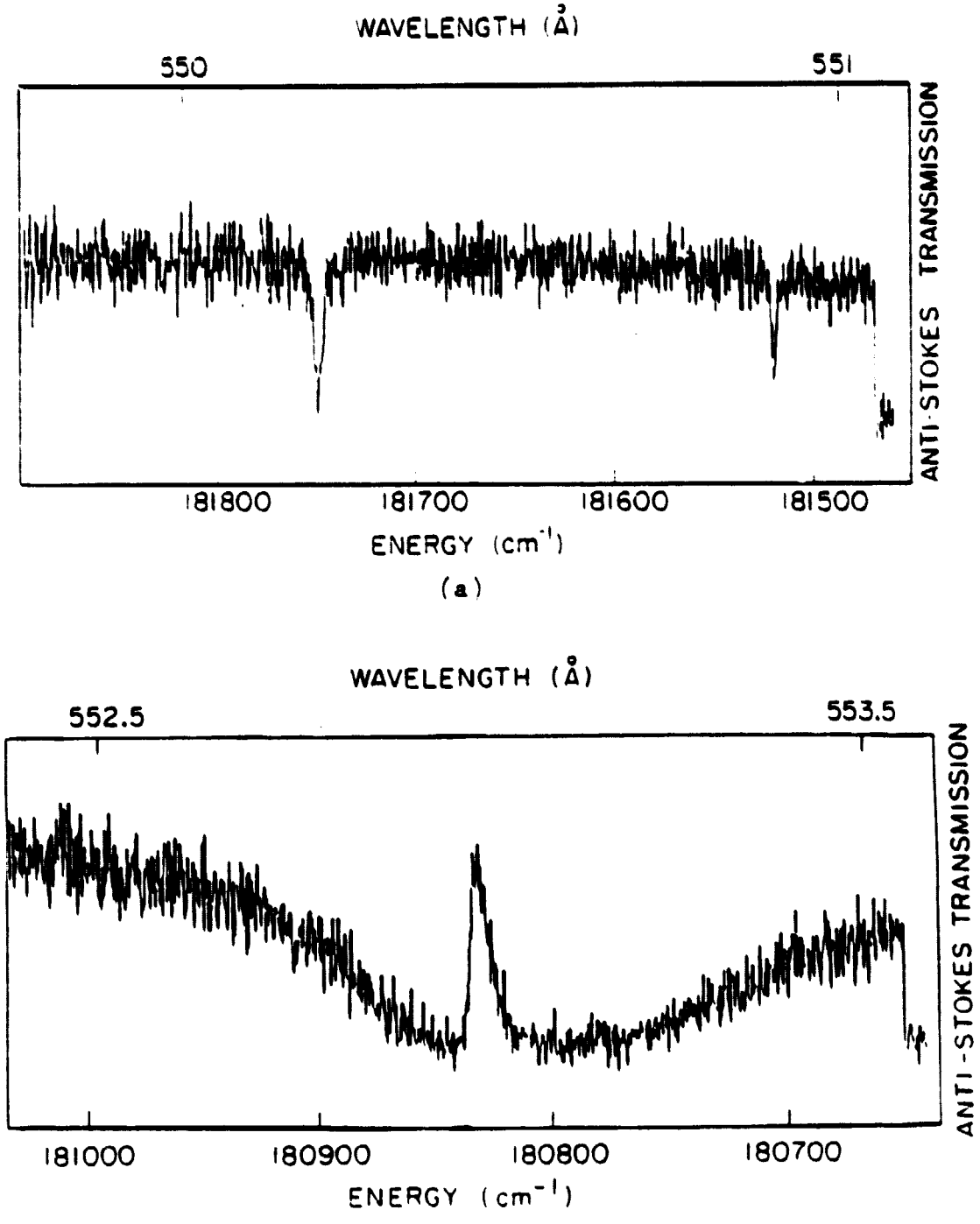

Fig. 8--Absorption scans of potassium obtained with microwave apparatus. Potassium cell length was 4.5 cm.
(a) Potassium vapor density was 1.0×10^{15} atoms/cm^3.
(b) Potassium vapor density was 2.2×10^{15} atoms/cm^3.

wavelength settings separated by 0.18 Å. To reduce the effects of background drifts, the computer rapidly scanned the laser wavelength and recorded the collected XUV flux level at each laser wavelength setting. At the end of each scan the laser was blocked to determine the background level. The plots of Fig. 8 represent the sum of 50 such scans, each one having only one laser pulse at each laser wavelength setting. The 50 scans took about 1-1/2 hours to complete.

Figure 8(a) shows two fairly narrow features at 181745 cm^{-1} and 181519 cm^{-1}, while Fig. 8(b) shows two broad, asymmetric features centered at 180794 cm^{-1} and 180840 cm^{-1} separated by a narrow ~ 100% transmission window. (The transmission level at the right end of the scan is reduced by an additional feature at 180547 cm^{-1}, beyond the range of the displayed scan.) The two (somewhat saturated) absorption features in Fig. 8(b) have very asymmetric profiles due to a strong interference between two discrete levels lying nearby in a single continuum. A complete cancellation of absorption cross section between two levels can be explained in terms of a Beutler-Fano [23] profile, and a simple analysis yields the ratio of the absorption cross section to the underlying continuum cross section. The values of the linewidths given in Table 5 for these levels were obtained by fitting absorption data taken at lower density, shown in Fig. 9, to the theoretical results. The theoretical calculation is represented by the solid line.

Highly asymmetric features such as these are somewhat rare in this region of the potassium absorption spectrum because of the small background photoionization cross section [24]. The Fano lineshape parameter q for a single discrete state in a continuum is then very large (typically 30 - 50 in potassium), and hence, the lineshape function is quite symmetric. In the

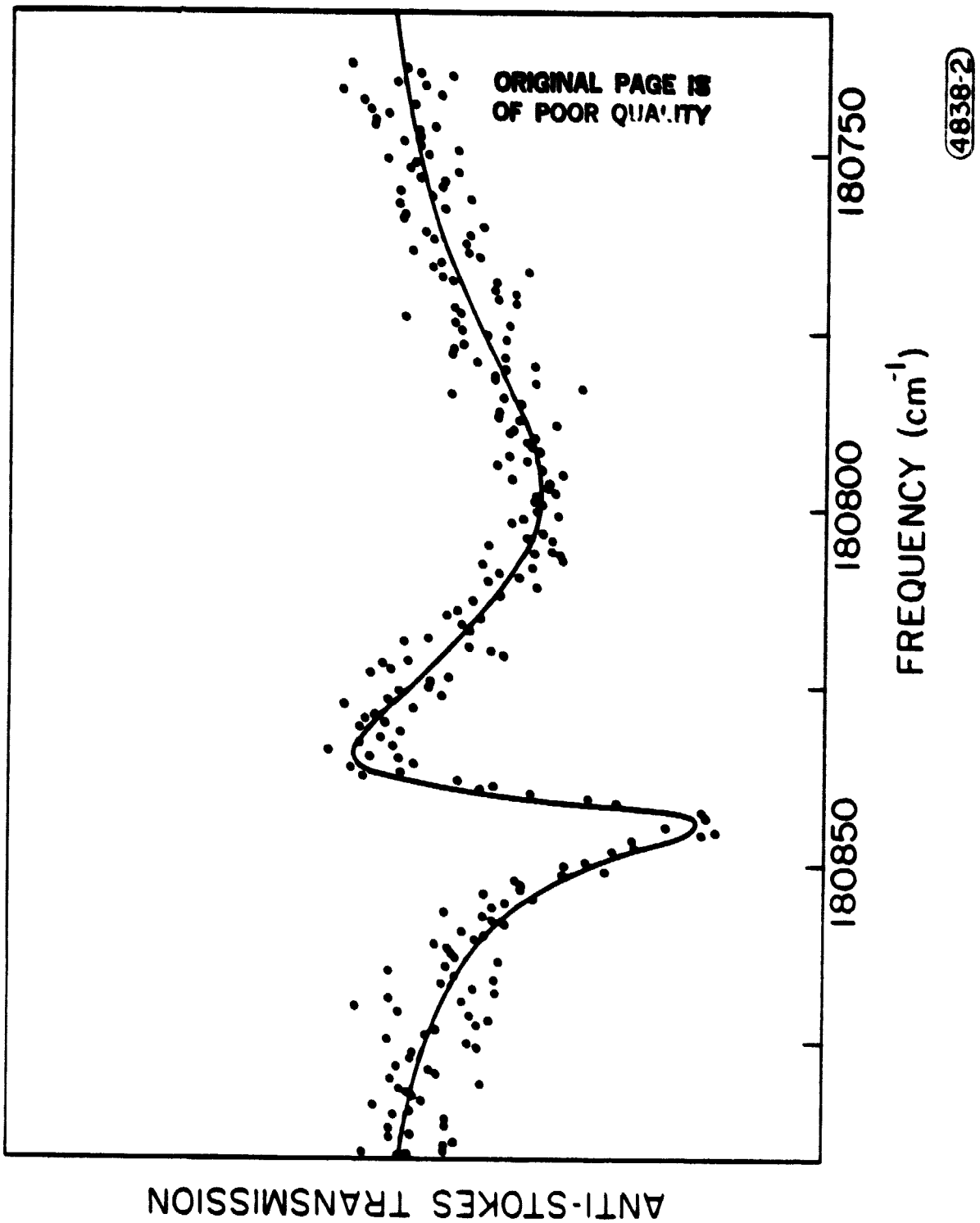

Fig. 9--Fit of theoretical Fano profile to potassium absorption data.

case discussed above, with two discrete states lying nearby, one can visualize the autoionization wing of one state as increasing the "background" photoionization cross section the other state sees. The q parameter of this state is thereby reduced, resulting in a very asymmetric lineshape. This intuitive approach is confirmed by the more exact result shown in Fig. 9.

IV. EXTENSION TO OTHER SYSTEMS

Using helium as the storage medium, the coverage of the spontaneous Raman anti-Stokes radiation source is limited by practical tunable lasers to the spectral region from approximately 537 Å to 584 Å. To access other spectral regions one must use different storage levels or other species.

Table 6 and Fig. 10 show how the other inert gases might be used to allow coverage of new spectral regions. In all of the inert gases, except for helium, the state of primary metastability has a total angular momentum of $J = 2$ and is also of opposite parity to that of the ground level [25]. In order to use these lowest metastable levels for anti-Stokes scattering one must therefore use a low power fixed frequency laser to resonantly transfer the population to a level of the same parity as ground and then use an intense tunable laser to generate the lower spontaneous Raman sideband. The $J = 1$ intermediate level will resonantly enhance the scattering cross section for this lower sideband.

Table 6 notes the primary storage level in each of the inert gases, the wavelength of the weak transfer laser, the center wavelength of the strong tunable laser, and the center wavelength of the emitted XUV radiation. The final column of this table notes the Doppler width for each of the species at $300^{\circ}K$.

Table 7 shows how the alkali ions might be used in an iso-electronic analogy to the noble atoms in Table 6. The Na II system which is iso-electronic to neon is shown in Fig. 11. We note that spontaneous anti-Stokes scattering in Li II has been observed by Willison, et al. [26].

One difference in using the iso-electronic column I ion is that the primary storage level may be populated by creating a core shell hole by

Table 6

Spontaneous Raman Scattering in the Inert Gases

Element	Metastable Level	Weak Transfer Laser Wavelength (Å)	Center Tunable Laser Wavelength (Å)	Center XUV Wavelength (Å)	Doppler Width (cm^{-1}) at 300°K
He	$1s2s\ ^1S$	--	5015 20581	537 584	1.15 1.06
Ne	$2p^5(^2P^o_{3/2})3s_{J=2}$	5944	6680	736	0.375
Ar	$3p^5(^2P^o_{3/2})4s_{J=2}$	7067	8408	1048	0.187
Kr	$4p^5(^2P^o_{3/2})5s_{J=2}$	5564	8266	1165	0.116
Xe	$5p^5(^2P^o_{3/2})6s_{J=2}$	4526 9048	8349 9926	1296 1470	0.0835 0.0736

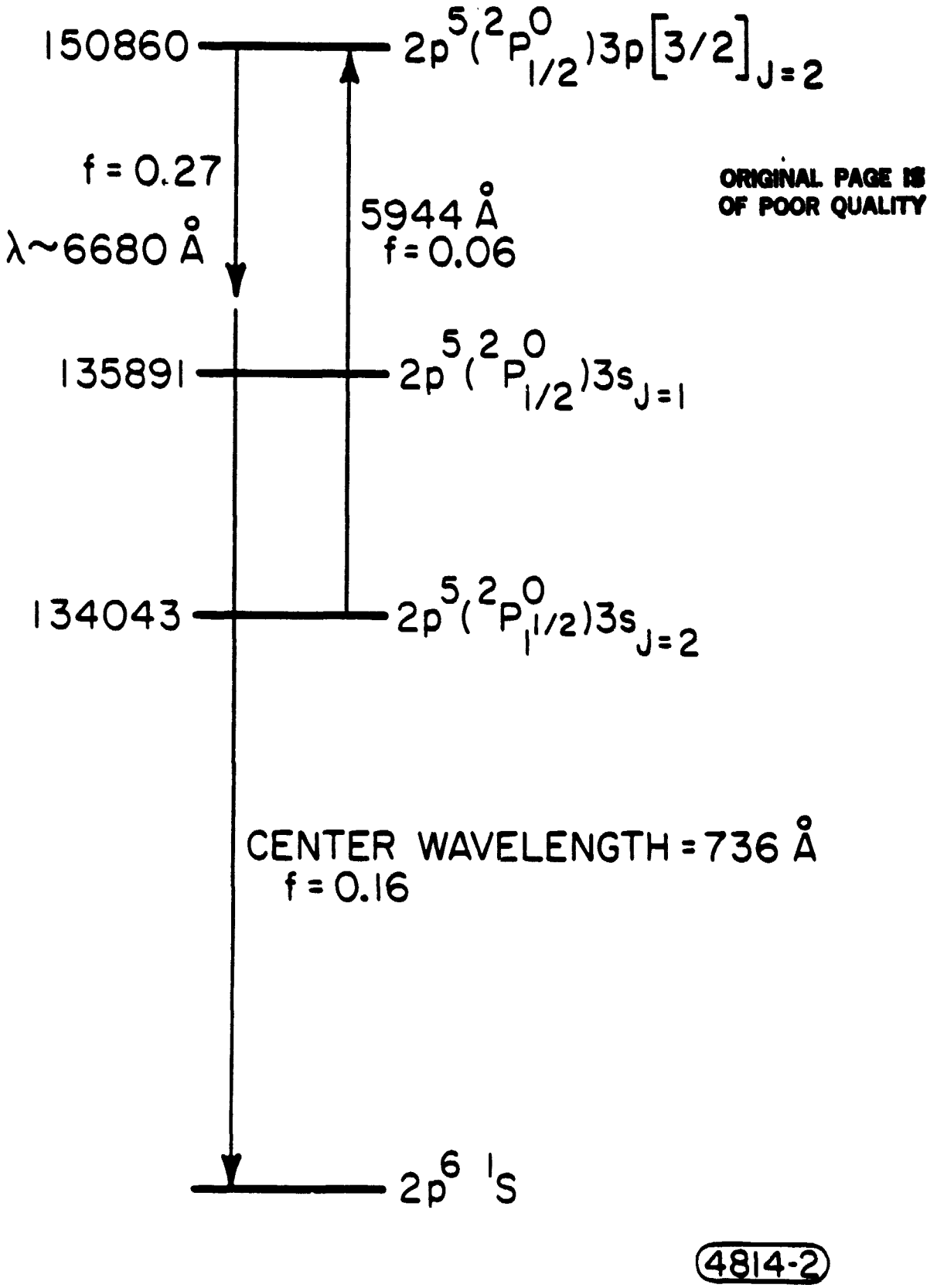

Fig. 10--Atomic energy level diagram showing spontaneous Raman scattering in neon.

Table 7

Spontaneous Raman Scattering in the Alkali Ions

Element	Metastable Level	Weak Transfer Laser Wavelength (Å)	Center Tunable Laser Wavelength (Å)	Center XUV Wavelength (Å)	Doppler Width (cm^{-1})	Temperature (^{o}K)
Li II	$1s2s\ ^{1}S$	--	9584	199	4.6	1150
Na II	$2p^{5}(^{2}P^{o}_{3/2})3s_{J=2}$	2843	3191	372	1.13	800
K II	$3p^{5}(^{2}P^{o}_{3/2})4s_{J=2}$	3683	4310	601	0.504	700
Rb II	$4p^{5}(^{2}P^{o}_{3/2})5s_{J=2}$	3162	4650	697	0.283	650
Cs II	$5p^{5}(^{2}P^{o}_{3/2})6s_{J=2}$	2778 4832	4871 4954	814 927	0.187 0.164	600

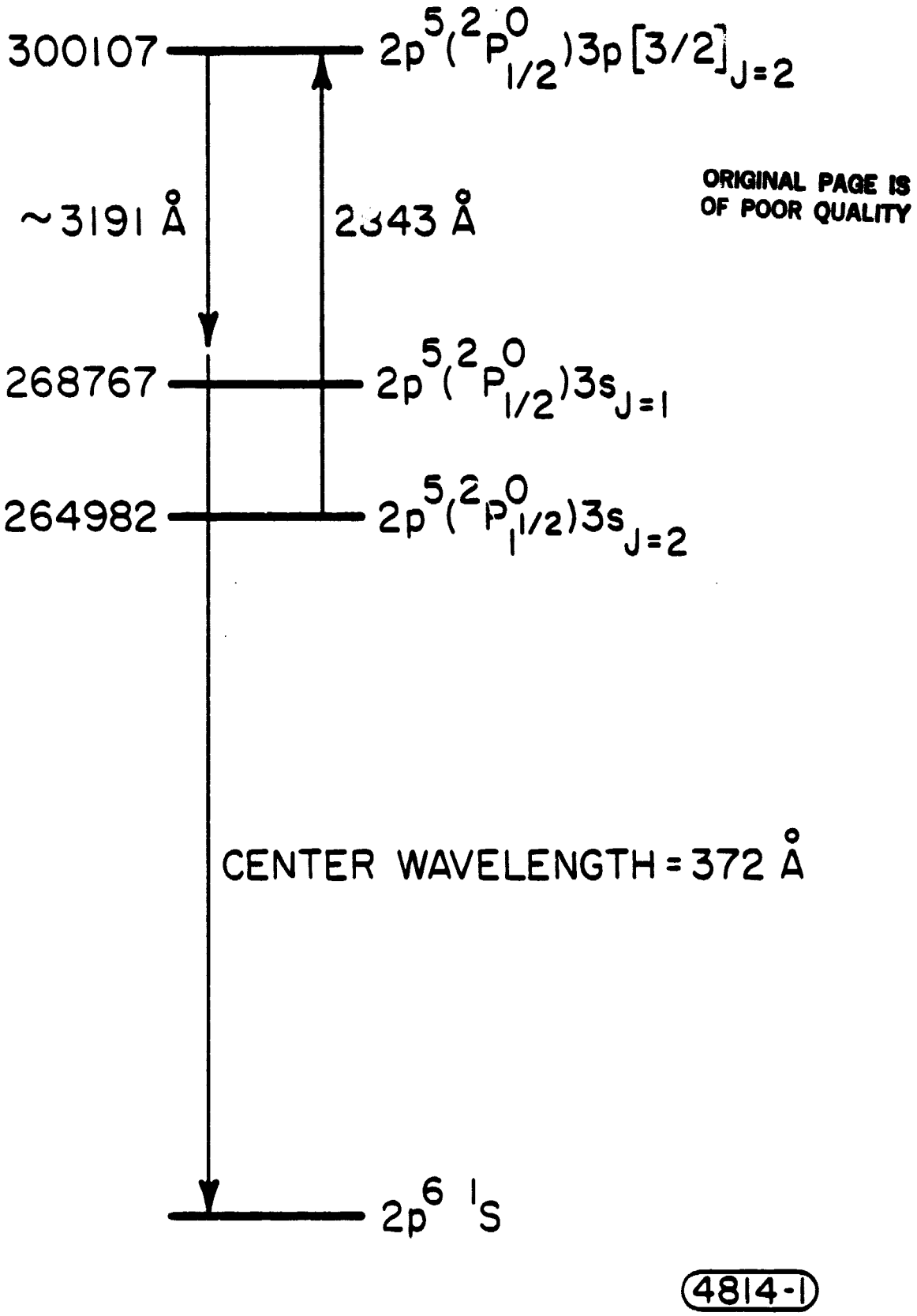

Fig. 11--Atomic energy level diagram showing spontaneous Raman scattering in Na^+.

photoionization. In recent experiments, Carlo, et al. [8] have used photoionization to produce populations as large as 3×10^{15} ions/cm^3 in the helium-like Li^+ triplet metastables.

If we assume that a frequency interval of 10,000 cm^{-1} can be attained with each of the Raman systems listed in Tables 6 and 7, then the total spectral range accessible to the anti-Stokes radiation source would be that shown in Fig. 12. This represents approximately 25% of the frequency interval from 200 Å to 1500 Å and approximately 75% of the interval from 500 Å to 1500 Å.

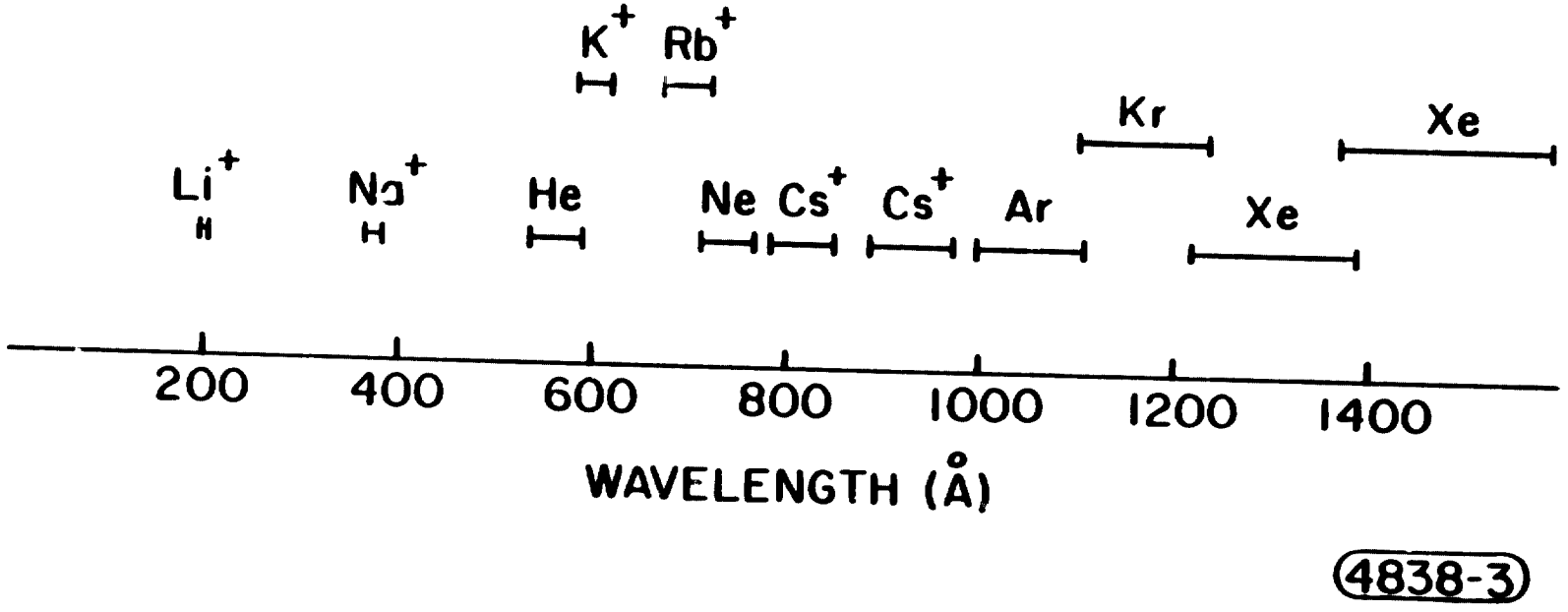

Fig. 12--Possible spectral regions which could be examined using the spontaneous Raman source.

V. CONCLUSION

The experiments described in this paper have shown that the spontaneous Raman anti-Stokes radiation source may be used to obtain very high resolution over limited spectral regions. The complexity of changing the storage species will limit the source to situations where features have been previously identified with lower resolution apparatus. Very often it is the case that the center wavelength which is obtainable from an ionic species, for example, 601 Å from K II (Table 7), coincides with the region of most interest for studying the core-excited spectrum of the neutral species. For example, if one is able to obtain ± 15,000 cm^{-1} of tuning centered at 601 Å, this would cover the spectral region from 551 Å to 660 Å. This would allow examination of a good portion of the interesting spectral region of K I.

Other properties of the spontaneous Raman anti-Stokes radiation source which may be useful are its controlled polarization and the ability to produce pulses as short as that of the incident laser.

The ultimate usefulness of this source will depend on the development of convenient methods for producing large metastable populations. Two promising approaches are the pulsed hollow cathode technology demonstrated by Falcone, et al. [7] and metastable production by photoionization with laser produced soft x-rays [8].

ACKNOWLEDGEMENTS

The authors gratefully acknowledge contributions to this work by E. Kintzer and D. Holmgren, and technical assistance by B. Yoshizumi. J. E. Rothenberg also gratefully acknowledges the support of the Fannie and John Hertz Foundation.

REFERENCES

[1] M. L. Ginter, D. S. Ginter, and C. M. Brown, "Need for high resolution in VUV Rydberg state spectroscopy," Appl. Opt., vol. 19, pp. 4015-4020, Dec. 1980.

[2] S. E. Harris, "Spontaneous anti-Stokes scattering as a high-resolution and picosecond-time-scale VUV light source," Appl. Phys. Lett., vol. 31, pp. 498-500, Oct. 1977.

[3] Joshua E. Rothenberg, J. F. Young, and S. E. Harris, "High-resolution extreme-ultraviolet spectroscopy of potassium using anti-Stokes radiation," Opt. Lett., vol. 6, pp. 363-365, Aug. 1981.

[4] R. W. Falcone, J. R. Willison, J. F. Young, and S. E. Harris, "Measurement of the He $1s2s\ ^1S_0$ isotopic shift using a tunable VUV anti-Stokes light source," Opt. Lett., vol. 3, pp. 162-163, Nov. 1978.

[5] P. Bräunlich and P. Lambropoulos, "Detection of singly stimulated two-photon emission from metastable deuterium atoms," Phys. Rev. Lett., vol. 25, pp. 135-318, July 1970; and "Anti-Stokes Raman scattering from metastable deuterium atoms," Phys. Rev. Lett., vol. 25, pp. 986-987, Oct. 1970.

[6] L. J. Zych, J. Lukasik, J. F. Young, and S. E. Harris, "Laser-induced two-photon blackbody radiation in the vacuum ultraviolet," Phys. Rev. Lett., vol. 40, pp. 1493-1496, June 1978.

[7] R. W. Falcone and K. D. Pedrotti, "Pulsed hollow-cathode discharge for extreme-ultraviolet lasers and radiation sources," Opt. Lett., vol. 7, pp. 74-76, Feb. 1982.

[8] R. G. Caro, J. C. Wang, R. W. Falcone, J. F. Young, and S. E. Harris, "Soft x-ray pumping of metastable levels of Li^{+}," Appl. Phys. Lett., vol. 42, pp. 9-11, Jan. 1983.

[9] V. L. Jacobs and J. Mizuno, "Interaction of laser light with the 2^1S_0 metastable state of helium," J. Phys. B: Atom. Molec. Phys., vol. 5, pp. 1155-1159, June 1972.

[10] E. Courtens and A. Szöke, "Time and spectral resolution in resonance scattering and resonance fluorescence," Phys. Rev. A, vol. 15, pp. 1588-1603, April 1977.

[11] Yu. M. Kagan and A. S. Taroyan, "Excitation of helium in a hollow cathode discharge – Part 1," Opt. Spect., vol. 35, pp. 120-123, Aug. 1973.

[12] G. N. Steele, "XUV filters: Out of this world and back again," Opt. Spectra, vol. 10, pp. 37-40, June 1976.

[13] R. B. Cairns and J. A. R. Samson, "Metal photocathodes as secondary standards for absolute intensity measurements in the vacuum ultraviolet," J. Opt. Soc. Amer., vol. 56, pp. 1568-1573, Nov. 1966.

[14] G. Herzberg, "Ionization potentials and Lamb shifts of the ground states of ^4He and ^3He," Proc. Roy. Soc. London A, vol. 248, pp. 309-332, Nov. 1958.

[15] W. C. Martin, "Energy levels and spectrum of neutral helium (^4He I)," J. Res. Nat. Bur. Stand., vol. 64A, pp. 19-28, Jan.-Feb. 1960.

[16] M. W. D. Mansfield, "The K I absorption spectrum in the vacuum ultraviolet: 3p-subshell excitation," Proc. Roy. Soc. London A, vol. 346, pp. 539-553, Nov. 1975.

[17] M. W. D. Mansfield and T. W. Ottley, "The identification of low energy K and Ca^+ autoionizing levels observed in electron impact experiments," Proc. Roy. Soc. London A, vol. 365, pp. 413-424, March 1979.

[18] G. Kavei, T. W. Ottley, V. Pejcev, and K. J. Ross, "High resolution ejected-electron spectra of K I and K II autoionizing levels excited by low-energy electron impact on potassium vapor," J. Phys. B: Atom. Molec. Phys., vol. 10, pp. 2923-2933, Oct. 1977.

[19] V. S. Borodin and Yu. M. Kagan, "Excitation of helium in a hollow-cathode discharge," Opt. Spect., vol. 23, pp. 108-110, July 1967.

[20] Joshua E. Rothenberg and Stephen E. Harris, "XUV lasers by quartet to doublet energy transfer in alkali atoms," IEEE J. Quantum Electron., vol. QE-17, pp. 418-422, March 1981.

[21] J. C. Wang and R. Normandin, unpublished data.

[22] T. Sasaki, H. Fukutani, K. Ishiguro, and T. Izumitani, "Determination of optical constants of glasses in the vacuum ultraviolet region," Japanese J. Appl. Phys., vol. 4, supplement 1, pp. 527-531, 1965.

[23] U. Fano, "Effects of configuration interaction on intensities and phase shifts," Phys. Rev., vol. 124, pp. 1866-1878, Dec. 1961.

[24] R. D. Hudson and V. L. Carter, "Experimental values of the atomic absorption cross section of potassium between 580 Å and 1000 Å," J. Opt. Soc. Amer., vol. 57, pp. 1471-1474, Dec. 1967.

[25] R. S. Van Dyck, Jr., C. E. Johnson, and H. A. Shugart, "Lifetime lower limits for the $^3P_0$ and $^3P_2$ metastable states of neon, argon, and krypton," Phys. Rev. A, vol. 5, pp. 991-993, Feb. 1972.

[26] J. R. Willison, R. W. Falcone, J. F. Young, and S. E. Harris, "Laser spectroscopy of metastable extreme-ultraviolet levels in lithium atoms and ions," Phys. Rev. Lett., vol. 47, pp. 1827-1829, Dec. 1981.